Title	Uniaxial flicker analysis of the psychophysical Stiles–Crawford effects
Authors(s)	Lochocki, Benjamin, Vohnsen, Brian
Publication date	2017-02-21
Publication information	Lochocki, Benjamin, and Brian Vohnsen. "Uniaxial Flicker Analysis of the Psychophysical Stiles–Crawford Effects." Taylor & Francis, February 21, 2017. https://doi.org/10.1080/09500340.2016.1237683.
Publisher	Taylor & Francis
Item record/more information	http://hdl.handle.net/10197/13057
Publisher's statement	This is an Accepted Manuscript of an article published by Taylor & Francis in Journal of Modern Optics on 21 February 2017, available online: http://www.tandfonline.com/10.1080/09500340.2016.1237683
Publisher's version (DOI)	10.1080/09500340.2016.1237683

DOI: https://doi.org/10.1080/09500340.2016.1237683

Uniaxial flicker analysis of the psychophysical Stiles-Crawford effects

Benjamin Lochocki[1,2] *and Brian Vohnsen*[1]

[1]Advanced Optical Imaging Group, School of Physics, University College Dublin, Dublin 4, Ireland

[2]Laboratorio de Óptica, Campus de Espinardo, Universidad de Murcia, 30100 Murcia, Spain

Email: benjamin@um.es

Corresponding author: *Benjamin Lochocki* Phone: 0034 868 888 555

Attributes (4 to 6 keywords)

Stiles-Crawford effect, photoreceptor cones, square-wave flicker, frequency dependence, directionality, hue shift

Abstract

Purpose: We report on a semi-automated system for frequency analysis of the Stiles-Crawford effect of the first kind (SCE-I) using flicker methodology designed to gain insight into the temporal dynamics of the perceived visibility for alternating pupil entrance points. We describe the system and its calibration in detail and discuss psychophysical measurement data obtained for the two authors.

Methods: A uniaxial system is used for SCE-I characterization of two emmetropic subjects as a function of flicker frequency for narrow wavelength bands chosen in the range of 450 to 700 nm using a fibre-guided tungsten-halogen lamp as light source. The flicker is realized using two orthogonally-mounted galvanometric scanning mirrors that allow linear trajectories at any angle across the pupil. A fast tuneable liquid crystal neutral-density filter is used for brightness adjustment and another liquid crystal filter is used for wavelength adjustment at each pupil point allowing simultaneous hue-shift determination for the Stiles-Crawford effect of the second kind (SCE-II).

Results: Validation of the system is realized with a CCD camera, a spectrometer, and a power meter and the data obtained are used in the software to calibrate all subsequent human subject measurements. The psychophysical data obtained show a strong frequency dependence of the Gaussian SCE-I with a characteristic directionality parameter, ρ, that is found to increase from $0.03/mm^2$ to $0.06/mm^2$ with flicker in the range of 1 to 10 Hz. The simultaneously determined hue shift could not be determined beyond 1 Hz due to the longer time required for a subjective determination.

Conclusion: We have reported on a fast uniaxial system for temporal characterization of the SCE-I. The psychophysical results obtained show that accurate specification of frequency in flicker analysis is mandatory when comparing SCE-I visibility and directionality curves obtained with those obtained using quasi-static bipartite fields. A uniaxial design offers unique advantages over that of common two-channel systems by completely eliminating spectral errors or brightness differences in the two branches that otherwise will impose on those of the visual system and degrade the psychophysical data. Future work with more subjects will be used to narrow the uncertainty and the causes of the effects observed.

1 Introduction

The Stiles-Crawford effect of the first kind (SCE-I) expresses a reduced visual sensitivity to light that enters the eye near to its pupil rim whereas the Stiles-Crawford effect of the second kind (SCE-II) expresses a simultaneous change in hue once the off-axis light has been subjectively corrected in brightness to counterbalance for the SCE-I (1–3). Both effects are commonly analysed using Maxwellian view of a quasi-static bipartite field with adjacent reference and test fields one of which is gradually adjusted in brightness and colour for a subjectively-determined match to the other. Alternatively, a flicker method with spatially overlapping reference and test fields can be used where only one is visible at a time and the brightness and wavelength of one (or the asymmetry of the flicker period) is adjusted until the flicker is no longer perceivable (1,4–6). A variant of the latter method is often used for incremental visibility determination where a flickering test light is positioned at the centre of a wider stationary reference field to allow incremental determination at the onset of flicker (7,8).

Temporal dynamics are known to influence the SCE-I and SCE-II. A sudden change in incidence angle at the retina when switching the entrance point to the diagonally opposite side of the pupil gives rise to a temporal increase in brightness termed the transient SCE-I (9). Likewise, a sudden change in polarization for light being incident towards the pupil rim gives rise to an increase in apparent brightness (10). Both effects diminish slowly over time until a steady state has been reached after approximately 40 sec. At a much faster pace, brightness changes can also be observed as a result of brief stimuli with vision recovery after approximately 100 ms following pulsed illumination (11,12). Bleaching alters the observed directionality (13) which is highest in objective studies of the related optical Stiles-Crawford effect (14–17). Here, we report on the analysis of the SCE-I at different time scales with flicker frequencies from 1.0 to 10 Hz where the latter coincides with the time needed for recovery following pulsed illumination.

A two-channel SCE-I system is prone to errors caused by beam splitters and differences in the optical components used for the two channels that may induce minor brightness or spectral changes and confound psychophysical measurements (1–6). To eliminate this risk a uniaxial illumination is to be preferred where the beam can be switched rapidly between the reference and test pupil entrance points while maintaining the appropriate settings of brightness and wavelength for each case. This is the approach taken in this study. Additionally, the uniaxial system is used to characterize the SCE-II although this can only be accomplished in the low-frequency limit. We report here on the technical characteristics of the developed system and discuss psychophysical measurement data obtained for the two authors.

2 Methods

The uniaxial flicker system and the experimental protocol implemented are described in the following.

2.1 Experimental Setup

A rapid uniaxial flicker system has been developed using a tungsten-halogen lamp as light source coupled to a coherent fibre bundle (NA = 0.22) with an exit diameter of 1.6 mm that is projected and reduced to 0.2 mm in the pupil plane of the subject using achromatic doublet lenses. The defocus of the subject at any tested wavelength is adjusted using a current-driven focal tuneable lens (Optotune, EL-10-30 LD, f_1 = 45-120 mm) mounted adjacent (at a central distance of 10 mm) to a negative achromatic lens (f_2 = -75 mm) (18) whereby a combined corrective range from -4 to +12 dioptres is obtained. The setup is shown schematically in Fig. 1. The iris which is placed at 4 mm from the vertical scanning mirror is imaged with unit magnification via a telescope (both with f = 40 mm) onto the horizontal scanning mirror. This is reimaged via the combination of the tuneable lens, f_2 and the eye onto the retina. The sharp edge of the imaged iris seen by the subject is used for gaze fixation and best in-focus viewing at each selected wavelength setting.

A tuneable liquid-crystal bandpass filter (Meadowlark, TOF-SB-VIS), LC colour filter, is used to adjust the wavelength and bandwidth of the illumination for any pupil entrance point (wavelength resolution is 0.1 nm and switching speed is ~100 ms) and a tuneable liquid crystal attenuator (Meadowlark, LVA-100-λ), LC ND, is used to adjust the brightness for each pupil entrance point (highest nominal contrast ratio is 500:1 and switching speed is ~0.25 ms). The liquid-crystal filters have been calibrated in the system using respectively a spectrometer (Ocean Optics USB2000) and powermeter (Thorlabs PM120D) in the plane of the eye pupil. Both liquid-crystal filters have orthogonally mounted polarizers incorporated at their entrance and exit faces, respectively, whereby the light remains linearly polarized throughout the system outside of the filters for any wavelength and attenuation. In all cases the light enters the eye with vertical linear polarization to ensure that the psychophysical measurements are unaffected by possible changes caused by ocular birefringence or transient polarization-sensitive responses of the visual pigments (10).

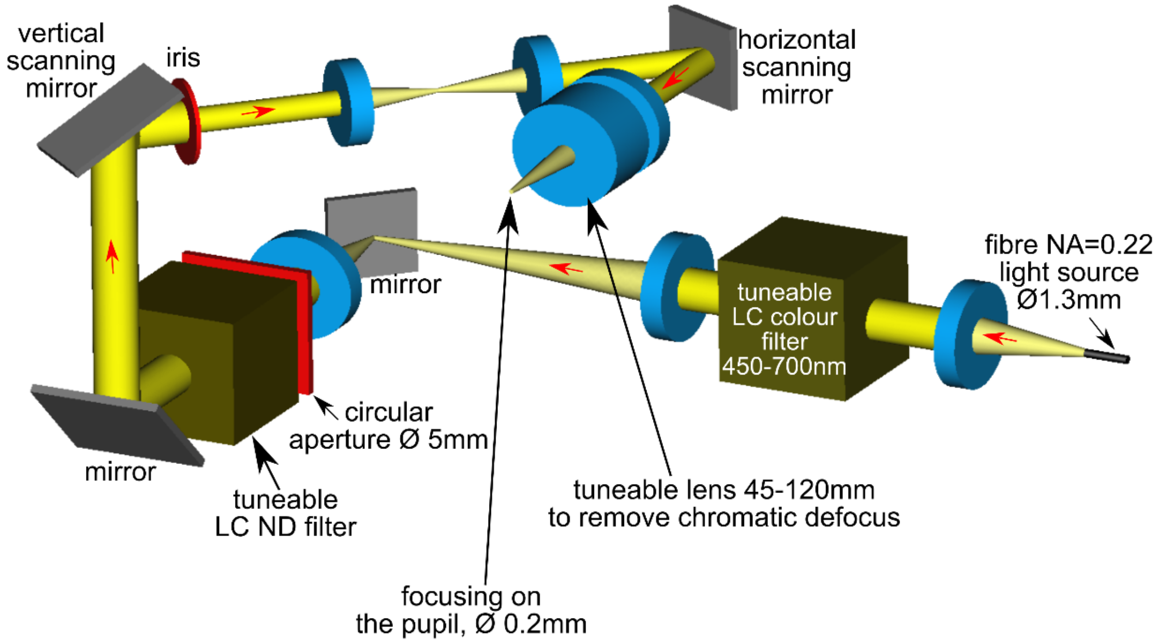

Fig. 1. Uniaxial beam-flickering system with liquid-crystal colour and neutral density filters, two galvanometric scanning mirrors and a current-driven tuneable lens for subjective defocus correction at any set wavelength. A circular aperture is used to prevent unwanted light to enter the ND filter and cause scattering but the limiting viewing angle is set by the smaller iris. The iris and the horizontal scanning mirror are located in conjugated retinal image planes.

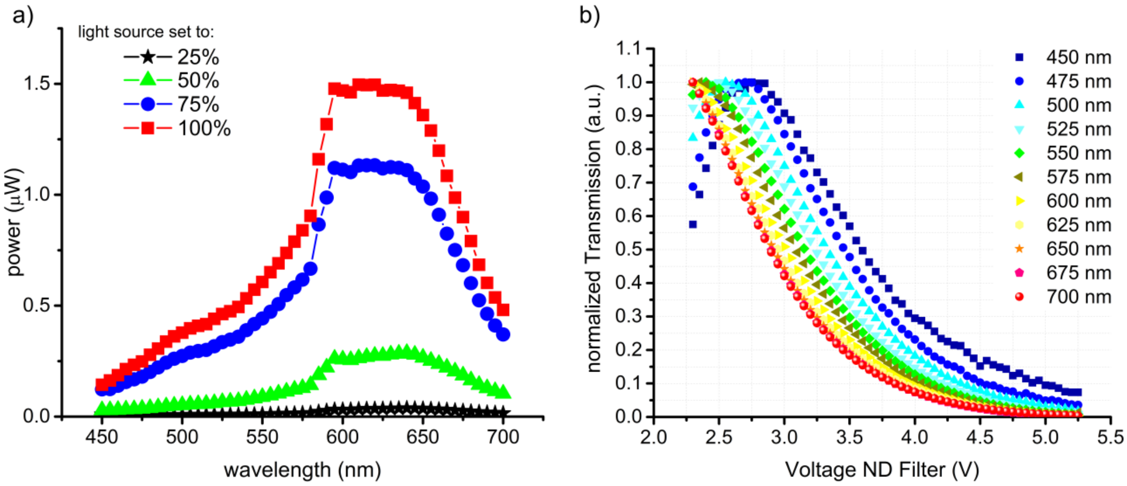

Fig. 2. (a) Optical power of the light being incident on the eye pupil for 4 different brightness settings of the light source. (b) Normalized calibration curves of the LC ND filter for each of the chosen LC colour narrowband wavelengths.

Fig. 2(a) shows the emission spectrum from the light source measured in the pupil plane (prior to insertion of the LC colour filter) for 4 different brightness settings. At high power settings the peak shifts slightly towards lower wavelengths as characteristic of the thermal emission. Since the LC colour filter picks out a narrow spectral window of this spectrum, with a bandwidth as shown in Fig. 4(b), the subject never sees the full range. For all of the psychophysical measurements the source was set at 50% with the exception of data taken at 450 and 475 nm wavelength where 75% was used to compensate for the low emission at short wavelengths. At the eye the measured incident power is a few nW, depending on the chosen wavelength, and thus at the retina this corresponds to a low photopic range without bleaching. The normalized transmissions of the liquid crystal ND filter versus applied voltage for each of the chosen wavelengths are shown in Fig. 4(b). Each curve is fitted to an individual 5^{th} order polynomial function ($R^2 > 0.99$) that subsequently serves as a lookup table within a LabVIEW™ interface which also provides test pattern control, data collection and numerical analysis.

Scanning of the incident light across the pupil is realized with two galvanometric scanning mirrors (GSI VM500+ with a nominal small-step-time of 0.20 ms). The subject views a uniform circular disc of light as set by the iris in a Maxwellian view that covers approximately 1.5 visual degrees centred at the fovea. Using rapid flickering with the galvanometric scanners driven by a square-wave signal, the system switches periodically between the reference position near to the pupil centre (at the peak-of-visibility for the SCE-I) and the off-axis pupil entrance point being tested while automatically alternating brightness and wavelength settings of the tuneable liquid-crystal filters. Fig. 3 shows the linear fitting of the horizontal and vertical scanning mirror driver voltage (proportional to the angular deviation of the mirrors) as a function of the effective power of the tuneable lens in combination with the negative achromatic lens. The dependence shows the required voltage to maintain a 3.5 mm off-axis pupil entrance point as measured with the CCD camera and graph paper in the pupil plane. When tuning the focal length of the lens the point of the incident light in the pupil plane will translate but this is prevented by simultaneously altering the driving voltage for the mirrors to counteract the displacement. This produces the linear fit shown which has been incorporated into the software so as to maintain a specific pupil entrance point for any chosen lens power. Thus, prior to any SCE-I and SCE-II analysis the galvanometric scanners have been calibrated with respect to the scanning position in the pupil plane.

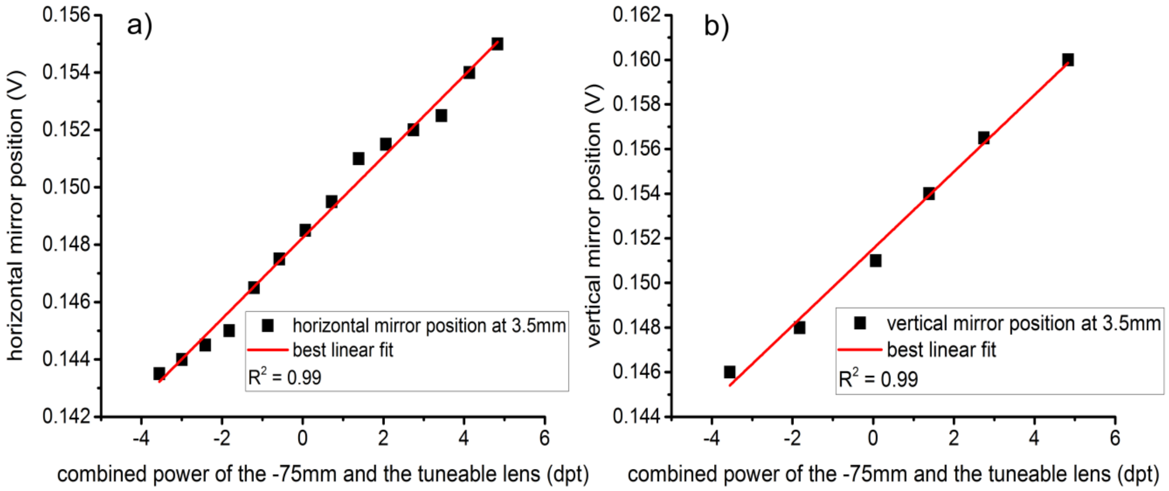

Fig. 3. Linear calibration curves for both galvanometric scanners: (a) horizontal scanning mirror and (b) vertical scanning mirror to maintain a +3.5 mm pupil entrance point. The correct mirror deflection depends on the combined lens power of the tuneable lens and the negative achromatic lens.

The brightness and central wavelength of the test light is adjusted in real time by the subject using a handheld gamepad until the best psychophysical match has been obtained between the spatially overlapping (but sequentially present) reference and test lights for any set flicker frequency (with an upper limit of 40 Hz). Thus, at any given instant the subject views only the reference or the test light. Once properly compensated in brightness and wavelength the flickering becomes unnoticeable as the transit time from reference to test pupil position is negligible without any ramping effects (<1 ms). At this stage the subject triggers the gamepad for recording of the subjectively determined visibility, defined as the ratio of intensity settings for the reference and test lights, prior to advancing to the next pupil point. The combination of two galvanometric scanners makes it possible to scan the pupil at any angle. It is expected that the directionality stemming from single photoreceptors is identical along any pupil traversal (19) although cone disarray within the viewing area may alter this ideal situation (17,20). Others have therefore analysed the psychophysical directionality in both horizontal and vertical pupil traverses but finding only small differences (on the order of 10%) in the two directions for red light at wavelengths of 620 nm (8) and 670 nm (7), respectively.

2.2 Experimental Procedure

Two emmetropic subjects (the authors) have been analysed in this study, BL (34y, left eye) and BV (44y, right eye). The eye pupil has been dilated and accommodation largely paralyzed using two drops of tropicamide (1%) repeated every 2 hours to maintain dilation throughout the experimental session. A bite bar was used to minimize unwanted head and eye motion. Procedures were approved by the Human Research Ethics Committee at University College Dublin.

Initially, each subject was centred with respect to the incident light at the SCE-I peak-of-visibility and the beam was gradually displaced across the dilated pupil both horizontally and vertically to ensure a proper alignment. Defocus at each tested wavelength was subjectively corrected using the current-tuneable lens until retinal displacement of the viewed test field as set by the iris had been eliminated for any pupil entrance point and test wavelength from 450 to 700 nm. This corresponds to the situation where the scanning mirrors are seen as being in focus by the subject. Subjective defocus calibration data are shown in Fig. 4(a). As can be noted both subjects reported a reduction in correction towards increasing wavelengths with the most significant changes occurring in the short wavelength limit in agreement with expectations based on the axial chromatic defocus of the human eye. Subject BV found the largest correction at 450 nm wavelength (although surprisingly also at 525 nm) possibly due to the reduced efficiency of the source, the low spectral sensitivity of the eye, or measurement uncertainty. As aberrations other than defocus are not being controlled, and the tuneable lens itself is also known to produce coma, these may explain some of the observed variations.

The implemented scan trajectory starts at the peak-of-visibility near the pupil centre and advances in a raster pattern in 0.5 mm steps across the pupil in 15 steps, equal to a total distance of 7.0 mm, until 4 complete pupil traverses have been completed. From these, average visibility values and standard deviations are determined at each sampled pupil point. The visibility is determined from the ratio of incident light power at any given pupil point with respect to the point of highest visibility. After the completion at a given wavelength, measurements were repeated across the spectrum at 11 set wavelengths (with an associated linear increase of bandwidth from 7 to 17 nm as seen in Fig. 4(b)) each corrected for subjective defocus. Finally, measurements were made at three different flickering frequencies of 1.0, 5.0, and 10 Hz. Data were collected for horizontal, vertical and oblique 45° traverses across the pupil. Measurements at each wavelength setting were completed in 5 to 10 min. and the total procedure at all wavelengths took approximately 4 hours with small breaks to avoid fatigue of the subject. Different flicker frequencies and pupil scanning directions were realized on separate days.

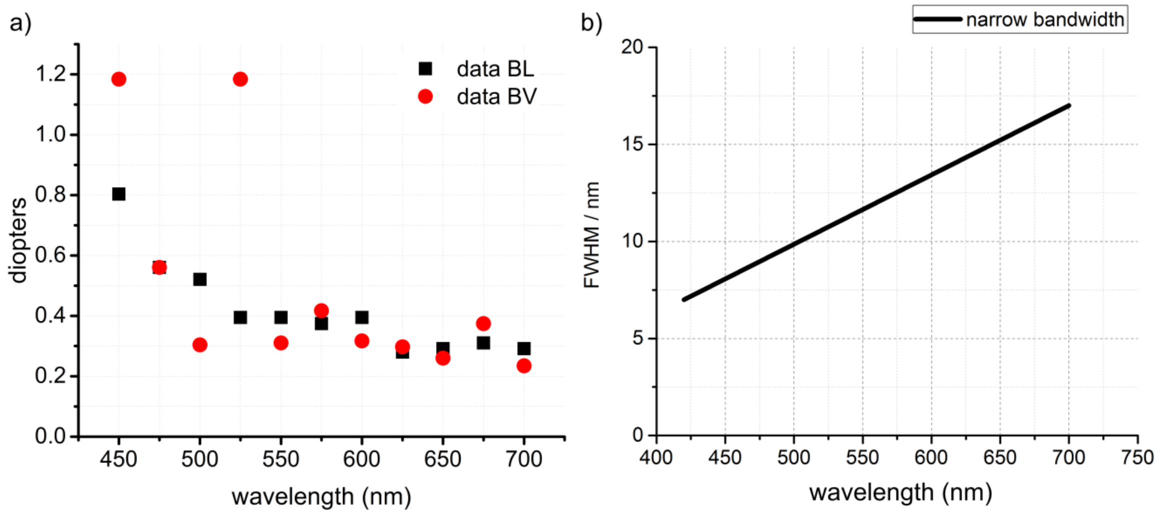

Fig. 4. (a) Individual defocus correction of the subject BL (black squares) and BV (red circles) as a function of wavelength setting using the current-driven focal tuneable lens in combination with the -75 mm negative achromatic lens, (b) Bandwidth at full-width-half-maximum using a narrow bandpass setting of the liquid-crystal bandpass filter as a function of the central wavelength.

3 Results and Discussion

Visibility data at each wavelength and flicker frequency were fitted to a Gaussian SCE-I function $\eta(x) = 10^{-\rho(x-x_0)^2}$, where x_0 represents the pupil location of the SCE-I peak-of-visibility and x denotes any point along the chosen axis of scanning across the pupil. Arbitrary points (x, y) along any specific pupil axis can be associated with a characteristic directionality parameter. Selected measurements at λ = 575 nm wavelength (narrow bandwidth setting of the liquid-crystal filter $\Delta\lambda$ = 12 nm) for both subjects are shown in Fig. 5 at the three tested frequencies. The directionality parameter and quality of each fit is indicated within the plots and it can be noted that the directionality parameter tends to increase with flicker frequency. Measurements at the other wavelengths (not shown for simplicity) resulted in very similar plots. All measurements fit a Gaussian SCE-I distribution with an R-squared value of 0.96 or higher.

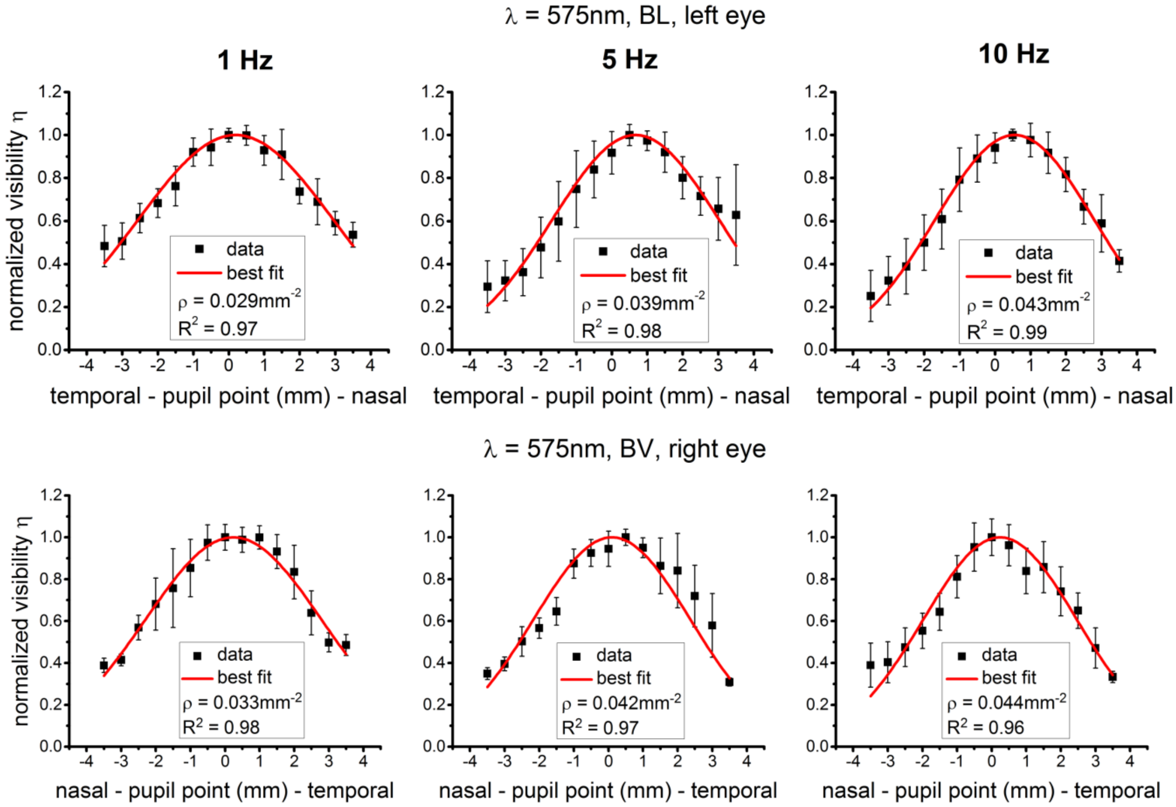

Fig. 5. Visibility curves of subjects BL and BV for the horizontal traverse using λ = 575 nm at 1, 5 and 10 Hz flicker frequencies. The red solid line is the best fit; the black squares represent the obtained data with standard-deviation error bars for a total of 8 pupil traverses. The directionality parameter ρ and R-squared values are indicated.

3.1 Spectral dependence of the SCE-I at different flicker frequencies

The directionality parameter determined across the analysed spectral range is shown in Fig. 6 revealing a slight increase with wavelength for both subjects at the three selected flicker frequencies and horizontal pupil traverses. A slight increase with wavelength is also found in most other cases when scanning either along a vertical axis or along a 45° diagonal as shown in Fig. 7 and Fig. 8 at three selected wavelengths. A minor increase in the characteristic SCE-I directionality parameter with wavelength differs from measurements of an objective Optical Stiles-Crawford effect where the characteristic directionality tends to lower with increasing wavelength (21) but it is well known that objective and subjective Stiles-Crawford directionality parameters differ (19,22) as one is based on the absorption of light in the outer-segment visual pigments whereas the other is related to directional backscattering of light from the retina. Although the SCE-I is only little affected by the absolute brightness of light in the photopic range (1) some impact of the spectral visibility curve of the eye cannot be ruled out in particular in the short-wavelength limit where the light is dimmer and the measurements are in the mesoscopic range. As this is foveal-only vision little impact is expected from parafoveal rods (that in any case show little directionality). A model based on depth-dependent absorption in the outer segments introduced by one of the authors (15) suggests a reduced directionality for dim light which may counter-balance the increased directionality at short wavelengths seen for retinal waveguide models and in the optical Stiles-Crawford effect (19,22) whereby the spectral dependence of the directionality becomes less marked.

Significant variations in the determined directionality can be observed at selected wavelengths but in terms of flicker frequency it can be seen that for both subjects the characteristic directionality tends to increase with flicker frequency. Table 1 shows the estimated directionality parameter based on linear fits of the data along the horizontal traverse at the 3 frequencies for the two subjects showing a small linear increase with wavelength with R-squared values in the range of 0.19 – 0.77. Most noteworthy, however, is that the observed directionality increases with flicker frequency from 1 to 10 Hz.

The ratio of the directionalities determined along the horizontal, vertical, and 45° traversals are shown in Table 2 having an average ratio of 1.006 ± 0.085. Thus, within experimental error they tend to be equal.

Table 1: Linear fit of directionality versus wavelength $\rho(\lambda)$ for the two subjects along the horizontal (0°) axis. The directionality is in 1/mm^2 units and the wavelength in µm. The adjusted R^2 is also indicated.

	BL	BV
1 Hz	0.02686 + 0.06736 (λ-0.55) $\overline{R}^2 = 0.579$	0.02602 + 0.03202 (λ-0.55) $\overline{R}^2 = 0.189$
5 Hz	0.03726 + 0.05319 (λ-0.55) $\overline{R}^2 = 0.720$	0.03931 + 0.06492 (λ-0.55) $\overline{R}^2 = 0.660$
10 Hz	0.04069 + 0.08602 (λ-0.55) $\overline{R}^2 = 0.774$	0.04495 + 0.09141 (λ-0.55) $\overline{R}^2 = 0.614$

Table 2: Ratio of determined directionality with standard deviation along the vertical (90°) and 45° pupil traverses with respect to the directionality along the horizontal (0°) axis at 3 wavelengths and 3 flicker frequencies for both subjects. The directionality is in 1/mm² units.

	ρ_{90}/ρ_0	ρ_{45}/ρ_0	ρ_{90}/ρ_0	ρ_{45}/ρ_0	ρ_{90}/ρ_0	ρ_{45}/ρ_0
	475 nm		575 nm		675 nm	
1 Hz (BL)	1.495 ± 0.141	0.984 ± 0.154	1.354 ± 0.173	0.975 ± 0.131	1.308 ± 0.112	1.004 ± 0.066
5 Hz (BL)	0.710 ± 0.104	0.767 ± 0.070	0.632 ± 0.093	0.903 ± 0.114	0.667 ± 0.097	0.772 ± 0.081
10 Hz (BL)	1.295 ± 0.158	1.272 ± 0.188	1.074 ± 0.150	1.306 ± 0.136	1.272 ± 0.135	1.195 ± 0.120
1 Hz (BV)	1.363 ± 0.123	1.161 ± 0.127	0.613 ± 0.060	0.887 ± 0.025	1.173 ± 0.104	1.267 ± 0.206
5 Hz (BV)	1.102 ± 0.105	0.731 ± 0.078	0.837 ± 0.066	0.753 ± 0.086	0.916 ± 0.061	1.012 ± 0.100
10 Hz (BV)	1.000 ± 0.099	0.688 ± 0.105	1.206 ± 0.137	0.907 ± 0.101	0.596 ± 0.078	1.004 ± 0.175

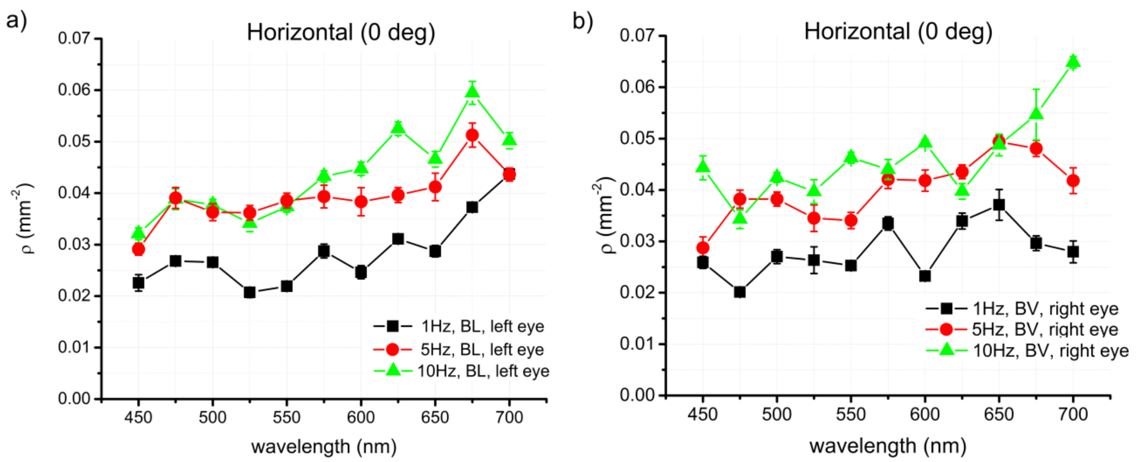

Fig. 6. Spectral dependence of the directionality parameter across the visible spectrum for the horizontal traverse of the subject (a) BL and (b) BV. Flicker frequencies are: 1 Hz (black squares), 5 Hz (red circles), and 10 Hz (green triangles). The error bars show the standard deviation of the obtained data.

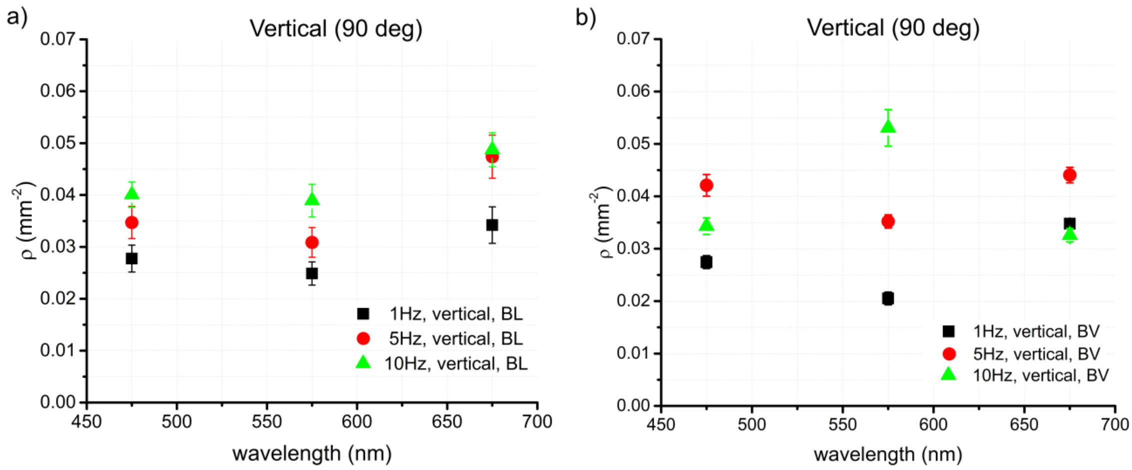

Fig. 7. Directionality parameter of the vertical traverse of the subject (a) BL and (b) BV. The error bars show the standard deviation of the obtained data.

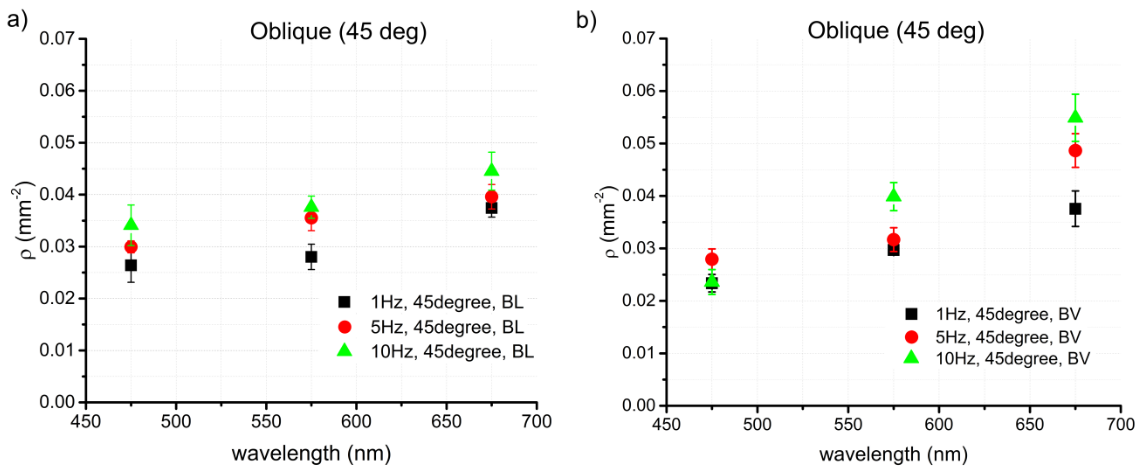

Fig. 8. Directionality parameter of the 45° traverse for subject (a) BL and (b) BV. The error bars show the standard deviation of the obtained data.

A number of authors have previously analysed the SCE-I with flicker methodologies reporting different results as summarized in Table 3. These are in fair agreement with those reported here but do not specifically target the temporal dependence of the directionality.

Table 3: SCE-I studies based on square-wave flicker analysis using mostly narrow-bandwidth incoherent light.

Authors	**Wavelength**	**Flicker frequency**	**Directionality parameter**
Applegate & Lakshminarayanan (7)	670 nm	2 Hz	0.048 – 0.053/mm^2
Singh, Atchison, Kasthurirangan & Guo (8)	620 nm	2 Hz	0.046/mm^2
Enoch (4)	552 nm	10 Hz	0.040/mm^2 (estimated)
He, Marcos & Burns (22)	543 nm (laser)	25 Hz	0.036 – 0.059/mm^2
Coble & Rushton (5,23)	580 nm	30 Hz	0.045/mm^2
Stiles & Crawford (1)	White light	"rapid rate"	(estimated) 0.05 – 0.08/mm^2
This study	450 – 700 nm	1, 5 and 10 Hz	0.020 – 0.065/mm^2

High frequency flicker can be detected even beyond 50 Hz by the human eye (24). As shown in this study, the rate of flicker is important when determining SCE-I directionality and should ideally be chosen above the critical flicker fusion rate to ease comparison with measurements obtained with a quasi-static bipartite field. At lower frequencies, the sensitivity of the eye peaks in the 8 – 10 Hz range (25,26) albeit when multiple frequencies are explored simultaneously different temporal channels become involved (27). A reduced directionality at low flicker frequencies can be understood from the aforementioned outer-segment absorption model (15). For oblique incidence of light pigments at one side of the outer segments are more exposed to light than those at the opposing side. This asymmetry due to self-screening gives the visual pigments at "the shadow side" time to recover until the direction of incidence is switched to the opposing side whereby the effective directionality is low. At high flicker rates this is no longer the case whereby the exposure becomes more symmetric by continuously activating the photo-isomeric process for all pigments across the exposed outer segments and the effective directionality increases. Trans-membrane diffusion of visual pigments could potentially occur between exposed and unexposed parts of outer segment membrane invaginations. In the case of rods, studies using frog outer segments have reported lateral diffusion coefficients of 2.5 μm^2/sec for photo-activated rhodopsin in the bilayer membrane disks which corresponds to a recovery time following bleaching on the order of ~10 s (28,29). This is significantly slower than the frequencies studied here and thus it is not likely to be a significant factor on the distribution of the pigments in the 0.1 to 1 s period of the flicker used.

3.2 The Stiles-Crawford effect of the second kind at three wavelengths

Using the same system, measurements where done where the subjects not only adjusted brightness to correct for the SCE-I but also wavelength of the test light using the liquid-crystal bandpass filter in incremental steps of $\Delta\lambda$ = 0.1 nm by means of the gamepad controller. The recorded wavelength shift is expected to be related to the observed hue shift while only quasi-monochromatic light is being used (30) and is shown in Fig. 7 for the central wavelength settings of 475, 575 and 675 nm using narrow and wide bandwidth settings of the filter, respectively. The fact that the SCE-I and SCE-II are centred at the same pupil point can be explained from the assumption that it relates to the derivative of the SCE-I visibility function (30). The largest shifts were observed with the larger bandwidth setting of the filter in agreement with the expectations. Observed hue shifts in the blue-green wavelength range were clearly marked but in the red where L-cones dominate the response only a small (BL) or negligible (BV) hue shift was observed. Some impact of the source spectrum shown in Fig. 2(a) is to be expected in particular at the 575 nm setting which is where the lamp emission spectra has the largest slope which may further enhance the apparent wavelength shift. This experiment could only be realized at low frequencies as the subjects could not clearly identify hues at a higher rate. It is noteworthy that subject BV did not experience any hue shift in the long wavelength limit of 675 nm wavelength and thus the narrow and wide bandwidth data coincides with zero hue shift. Although only two subjects were analysed it does show the potential of the developed system for semi-automated determination of both the SCE-I and SCE-II and their associated characteristics.

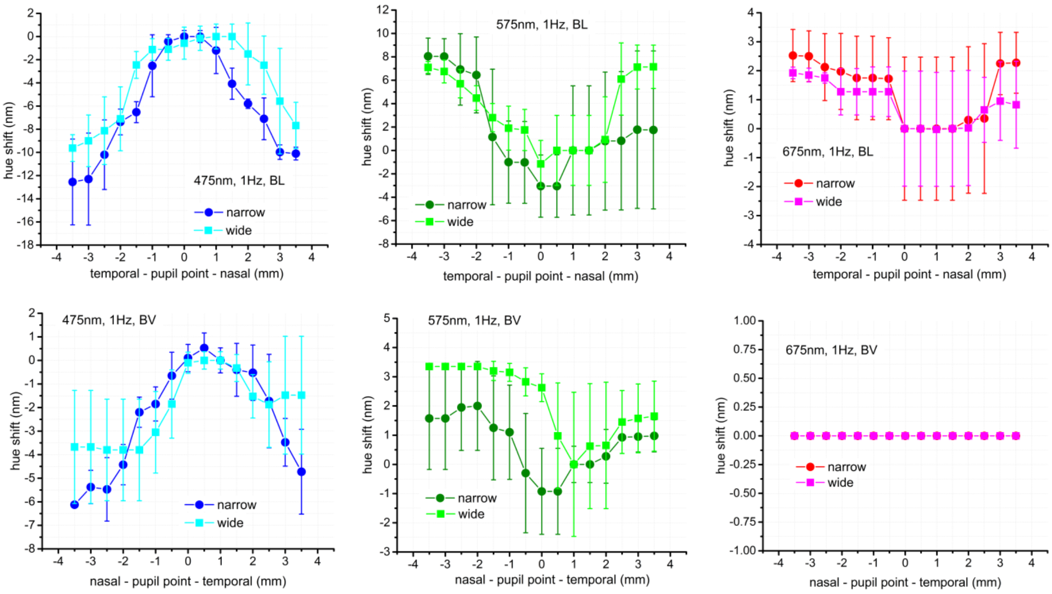

Fig. 9. Recorded wavelength shifts for best colour matching of the SCE-II in the horizontal pupil traverse for subject BL (top) and BV (bottom). Three wavelength settings of the liquid-crystal colour filter 475, 575, and 675 nm were used with narrow (dark coloured line) and wide (dark coloured line) bandwidth settings, respectively. The data were obtained with a flicker frequency of 1 Hz and error bars show standard deviations of the measured data. Note that subject BV did not observe any hue shift for 675 nm wavelength light neither for the narrow nor for the wide bandwidth setting.

It is important to stress that the measured wavelength shift has been determined with only one wavelength range of the source at a time (as set by the liquid-crystal colour filter) and thus a perfect match that takes into account also fractional absorption and bleaching of the three distinct visual pigments is beyond the scope of the present study. Fully trichromatic measurements have been realized by others although even in this case a perfect match across the visual field has not yet been obtained (31,32).

Conclusions

A single beam flickering system with Maxwellian illumination and synchronized tuneable liquid-crystal filters has been designed and used to measure the psychophysical SCE-I and SCE-II at different flicker frequencies for foveal vision with 2 subjects. The experimental results show an increase in directionality with flicker frequency and also a slight increase with wavelength using a uniaxial automated system that removes artefacts caused by instrumental differences with different illumination paths. The determined directionality with flicker becomes similar to that determined with conventional quasi-static bipartite fields in the high-frequency limit. At lower frequencies, pigments and visual sensation partially recovers after each illumination condition thus directly demonstrating a temporal component in the directional sensitivity of the retina (9,33,34). We are conducting further research with more subjects to narrow the uncertainty and gain deeper insight into the observed phenomena.

Acknowledgements

This research has been realized with financial support from the Irish Research Council and Science Foundation Ireland (grant: 08/IN.1/B2053).

References

1. W. S. Stiles and B. H. Crawford, "The luminous efficiency of rays entering the eye pupil at different points," Proc. R. Soc. London, Ser. B, Contain. Pap. a Biol. Character **112**, 428–450 (1933).

2. W. S. Stiles, "The luminous efficiency of monochromatic rays entering the pupil at different points and a new colour effect," Proc. R. Soc. London, Ser. B, Biol. Sci. **123**, 90–118 (1937).

3. B. Lochocki, D. Rativa, and B. Vohnsen, "Spatial and spectral characterisation of the first and second Stiles-Crawford effects using tuneable liquid-crystal filters," J. Mod. Opt. **58**, 1817–1825 (2011).

4. J. M. Enoch, "Summated response of the retina to light entering different parts of the pupil," J. Opt. Soc. Am. **48**, 392–405 (1958).

5. J. R. Coble and W. A. H. Rushton, "Stiles-Crawford effect and the bleaching of cone pigments," J. Physiol. **217**, 231–242 (1971).

6. G. Westheimer, "Directional sensitivity of the retina: 75 years of Stiles-Crawford effect," Proc. R. Soc. B, Biol. Sci. **275**, 2777–2786 (2008).

7. R. A. Applegate and V. Lakshminarayanan, "Parametric representation of Stiles-Crawford functions: normal variation of peak location and directionality," J. Opt. Soc. Am. A **10**, 1611–1623 (1993).

8. N. Singh, D. A. Atchison, S. Kasthurirangan, and H. Guo, "Influences of accommodation and myopia on the foveal Stiles-Crawford effect," J. Mod. Opt. **56**, 2217–2230 (2009).

9. W. Makous, "A transient Stiles-Crawford effect," Vision Res. **8**, 1271–1284 (1968).

10. P. J. de Groot, "Transient threshold increase due to combined changes in direction of propagation and plane of polarization," Vision Res. **19**, 1253–1259 (1979).

11. B. H. Crawford, "Visual adaptation in relation to brief conditioning stimuli," Proc. R. Soc. B Biol. Sci. **134**, 283–302 (1947).

12. J. Pokorny, V. C. W. Sun, and V. C. Smith, "Temporal dynamics of early light adaptation," J. Vis. **3**, 423–431 (2003).

13. P. L. Walraven, "Recovery from the increase of the Stiles-Crawford effect after bleaching," Nature **210**, 311–312 (1966).

14. S. A. Burns and A. E. Elsner, "Color matching at high illuminances: photopigment optical density and pupil entry," J. Opt. Soc. Am. A **10**, 221–230 (1993).

15. B. Vohnsen, "Directional sensitivity of the retina: A layered scattering model of outer-segment photoreceptor pigments," Biomed. Opt. Express **5**, 1569–1587 (2014).

16. S. A. Burns, S. Wu, F. Delori, and A. E. Elsner, "Direct measurement of human-cone-photoreceptor alignment," J. Opt. Soc. Am. A **12**, 2329–2338 (1995).

17. H. J. Morris, L. Blanco, J. L. Codona, S. L. Li, S. S. Choi, and N. Doble,

"Directionality of individual cone photoreceptors in the parafoveal region," Vision Res. **117**, 67–80 (2015).

18. B. Lochocki and B. Vohnsen, "Defocus-corrected analysis of the foveal Stiles-Crawford effect of the first kind across the visible spectrum," J. Opt. **15**, 125301 (2013).

19. B. Vohnsen, I. Iglesias, and P. Artal, "Guided light and diffraction model of human-eye photoreceptors," J. Opt. Soc. Am. A **22**, 2318–2328 (2005).

20. A. Safir and L. Hyams, "Distribution of cone orientations as an explanation of the Stiles-Crawford effect," J. Opt. Soc. Am. **59**, 757–765 (1969).

21. N. P. Zagers, T. T. Berendschot, and D. van Norren, "Wavelength dependence of reflectometric cone photoreceptor directionality," J. Opt. Soc. Am. A **20**, 18–23 (2003).

22. J. C. He, S. Marcos, and S. A. Burns, "Comparison of cone directionality determined by psychophysical and reflectometric techniques," J. Opt. Soc. Am. A **16**, 2363–2369 (1999).

23. C. Hood and W. A. H. Rushton, "The Florida retinal densitometer," J. Physiol. **217**, 213–229 (1971).

24. J. Davis, Y.-H. Hsieh, and H.-C. Lee, "Humans perceive flicker artifacts at 500 Hz," Sci. Rep. **5**, 1–4 (2015).

25. D. H. Kelly, "Visual response to time-dependent stimuli. I. Amplitude sensitivity measurements," J. Opt. Soc. Am. **51**, 422–429 (1961).

26. D. G. Green, "Sinusoidal flicker characteristics of the color-sensitive mechanisms of the eye," Vision Res. **9**, 591–601 (1969).

27. W. Makous, "Fourier models and the loci of adaptation," J. Opt. Soc. Am. A **14**, 2323–2345 (1997).

28. M. W. Kaplan, "Rhodopsin lateral diffusion as a function of rod outer segment disk membrane axial position," Biophys. J. **45**, 851–853 (1984).

29. Q. Wu, C. Chen and Y. Koutalos, "All-trans retinol in rod photoreceptor outer segments moves unrestrictedly by passive diffusion," Biophys. J. **91**, 4678–4689 (2006).

30. B. Vohnsen, "On the spectral relation between the first and second Stiles-Crawford effect," J. Mod. Opt. **56**, 2261–2271 (2009).

31. J. M. Enoch and W. S. Stiles, "The colour change of monochromatic light with retinal angle of incidence," Opt. Acta **8**, 329–358 (1961).

32. M. Alpern, "Lack of uniformity in colour matching," J. Physiol. (London) **288**, 85–105 (1979).

33. S. Castillo and B. Vohnsen, "Exploring the Stiles-Crawford effect of the first kind with coherent light and dual maxwellian sources," Appl. Opt. **52**, A1–A8 (2013).

34. D. I. A. MacLeod, "Directional selective light adaptation: a visual consequence of receptor disarray?," Vision Res. **14**, 369–378 (1973).